

# SPARSE CIRCULAR COORDINATES VIA PRINCIPAL $\mathbb{Z}$ -BUNDLES

JOSE A. PEREA

**ABSTRACT.** We present in this paper an application of the theory of principal bundles to the problem of nonlinear dimensionality reduction in data analysis. More explicitly, we derive, from a 1-dimensional persistent cohomology computation, explicit formulas for circle-valued functions on data with nontrivial underlying topology. We show that the language of principal bundles leads to coordinates defined on an open neighborhood of the data, but computed using only a smaller subset of landmarks. It is in this sense that the coordinates are sparse. Several data examples are presented, as well as theoretical results underlying the construction.

## 1. INTRODUCTION

The curse of dimensionality refers to a host of phenomena inherent to the increase in the number of features describing the elements of a data sets. For instance, in statistical learning, the number of training data points needs to grow roughly exponentially in the number of features, in order for learning algorithms to generalize correctly in the absence of other priors. A deeper manifestation of the curse of dimensionality is the deterioration of the concept of “nearest neighbors” in high-dimensional Euclidean space; for as the dimension increases, the distance between any two points is roughly the same [18]. One of the most popular priors in data science is the “low intrinsic dimensionality” hypothesis. It contends that while the apparent number of features describing each data point (e.g., the number of pixels in an image) might be large, the effective number of degrees of freedom (i.e., the intrinsic dimensionality) is often much lower. Indeed, images generated at random will hardly depict a cat or a natural scene.

Many dimensionality reduction schemes have been proposed in the literature to leverage the “low intrinsic dimensionality” hypothesis; each making explicit or implicit use of a likely characteristic of the data. For instance, Principal Component Analysis [10] and other linear dimensionality reduction methods, rely on the existence of a low-dimensional linear representation accounting for most of the variation in the data. Methods such as Locally Linear Embeddings [19] and Laplacian EigenMaps [2], on the other hand, presuppose the existence of a manifold-like object parametrizing the underlying data space. Other algorithms such as Multi-dimensional Scaling [11] and Isomap [22], attempt to preserve distances between data points, while providing low-dimensional reconstructions.

---

2010 *Mathematics Subject Classification.* Primary 55R99, 55N99, 68W05; Secondary 55U99.

*Key words and phrases.* Circular Coordinates, Persistent cohomology, Principal Bundles, Classifying Map.

This work was partially supported by the NSF under grant DMS-1622301 and DARPA under grant HR0011-16-2-003.

Recently, a host of new methods for nonlinear dimensionality reduction has emerged from the field of computational topology [6, 21, 17]. The idea being that if the underlying space from which the data has been sampled has a particular shape, then this information can be used to generate appropriate low-dimensional representations. The circular coordinates of de Silva, Morozov, and Vejdemo-Johansson [6], pioneered the use of persistent cohomology as a way to measure the shape of a data set, and then produce circle-valued coordinates reflecting the underlying nontrivial topology. Their algorithm goes as follows. Given a finite metric space  $(X, \mathbf{d})$ , the data, and a scale  $\alpha > 0$  so that the Rips complex

$$R_\alpha(X) := \{\sigma \subset X : \sigma \neq \emptyset \text{ and } \text{diam}(\sigma) < \alpha\}$$

has a nontrivial integer cohomology class  $[\eta] \in H^1(R_\alpha(X); \mathbb{Z})$  — this is determined from the persistent cohomology of the Rips filtration  $\mathcal{R}(X) = \{R_\epsilon(X)\}_{\epsilon \geq 0}$  — a linear least squares optimization (of size the number of vertices by the number of edges of  $R_\alpha(X)$ ) is solved, in order to construct a function  $f_\eta : X \rightarrow S^1 \subset \mathbb{C}$  which, roughly, puts one of the generators for  $H^1(S^1; \mathbb{Z})$  in correspondence with  $[\eta] \in H^1(R_\alpha(X); \mathbb{Z})$ .

**1.1. Our Contribution.** Two drawbacks of the perspective presented in [6] are: (1) the method requires a persistent cohomology calculation, as well as a least squares optimization, on the Rips complex of the entire data set  $X$ . This is computationally expensive and may limit applicability to small-to-medium-sized data. (2) once the function  $f_\eta$  has been computed, it is only defined on the data points from  $X$  used for its construction. In this paper, we show that these drawbacks can be addressed effectively with ideas from principal  $\mathbb{Z}$ -bundles. In particular, we show that it is possible to construct circular coordinates using a subset of landmarks  $L \subset X$ , with similar classifying properties as in [6], Theorem 3.3 and Proposition 4.3, and that said coordinates will be defined on an open neighborhood of  $L$  containing  $X$ . We call these functions “sparse circular coordinates”.

**1.2. The Sparse Circular Coordinates Algorithm.** Let us describe next the steps needed to construct said coordinates. The rest of the paper is devoted to the theory behind these choices:

- (1) Let  $(X, \mathbf{d})$  be the input data set; i.e. a finite metric space. Select a set of landmarks  $L = \{\ell_1, \dots, \ell_N\} \subset X$ , e.g. at random or via `maxmin` sampling, and let

$$r_L = \max_{x \in X} \min_{\ell \in L} \mathbf{d}(x, \ell)$$

be the radius of coverage.

- (2) Choose a prime  $q > 2$  at random and compute the persistent cohomology  $PH^1(\mathcal{R}(L); \mathbb{Z}/q)$  for the Rips filtration on  $L$ . Let  $\mathbf{dgm}(L)$  be the resulting persistence diagram.
- (3) If  $(a, b) \in \mathbf{dgm}(L)$  is so that  $\max\{a, r_L\} < \frac{b}{2}$ , then let

$$\alpha = t \cdot \max\{a, r_L\} + (1 - t) \frac{b}{2} \quad , \quad \text{for some } 0 < t < 1$$

Let  $\eta' \in Z^1(R_{2\alpha}(L); \mathbb{Z}/q)$  be a representative for the persistent cohomology class corresponding to  $(a, b) \in \mathbf{dgm}(L)$ . If  $t$  is closer to 1, then the circular coordinates are defined on a bigger domain; however, this makes step (5) below more computationally intensive.

- (4) Lift  $\eta' : C_1(R_{2\alpha}(L); \mathbb{Z}) \longrightarrow \mathbb{Z}/q = \{0, \dots, q-1\}$  to an integer cocycle  $\eta \in C^2(R_{2\alpha}(L); \mathbb{Z})$ . That is, one for which  $\eta' - (\eta \bmod q)$  is a coboundary in  $C^1(R_{2\alpha}(L); \mathbb{Z}/q)$ . An explicit choice (that works in practice for a prime  $q$  chosen at random) is the integer cochain:

$$\eta(\sigma) = \begin{cases} \eta'(\sigma) & \text{if } \eta'(\sigma) \leq \frac{q-1}{2} \\ \eta'(\sigma) - q & \text{if } \eta'(\sigma) > \frac{q-1}{2} \end{cases}$$

- (5) Choose positive weights for the vertices and edges of  $R_{2\alpha}(L)$  — e.g. all equal to 1 — and let  $d_{2\alpha}^+ : C^1(R_{2\alpha}(L); \mathbb{R}) \longrightarrow C^0(R_{2\alpha}(L); \mathbb{R})$  be the (weighted) Moore-Penrose pseudoinverse (solving weighted linear least squares problems) for the coboundary map

$$d_{2\alpha} : C^0(R_{2\alpha}(L); \mathbb{R}) \longrightarrow C^1(R_{2\alpha}(L); \mathbb{R})$$

If  $\iota : \mathbb{Z} \hookrightarrow \mathbb{R}$  is the inclusion, let

$$\tau = -d_{2\alpha}^+(\iota \circ \eta) \quad \text{and} \quad \theta = (\iota \circ \eta) + d_{2\alpha}(\tau)$$

- (6) Denote by  $\tau_j \in \mathbb{R}$  the value of  $\tau$  on the vertex  $\ell_j \in L$ , and by  $\theta_{jk} \in \mathbb{R}$  the value of  $\theta$  on the oriented edge  $[\ell_j, \ell_k] \in R_{2\alpha}(L)$ . If we let

$$\varphi_j(b) = \frac{|\alpha - \mathbf{d}(\ell_j, b)|_+}{\sum_{k=1}^N |\alpha - \mathbf{d}(\ell_k, b)|_+} \quad \text{where} \quad |r|_+ = \max\{r, 0\}, \quad r \in \mathbb{R}$$

and  $B_\alpha(\ell_k)$  denotes the open ball of radius  $\alpha > 0$  centered at  $\ell_k \in L$ , then the sparse circular coordinates are defined by the formula:

$$\boxed{\begin{aligned} h_\eta : \bigcup_{k=1}^N B_\alpha(\ell_k) &\longrightarrow S^1 \subset \mathbb{C} \\ B_\alpha(\ell_j) \ni b &\mapsto \exp \left\{ 2\pi i \left( \tau_j + \sum_{k=1}^N \varphi_k(b) \theta_{jk} \right) \right\} \end{aligned}} \quad (1)$$

If  $X$  is a subspace of an ambient metric space  $\mathbb{M}$ , then the  $B_\alpha(\ell_k)$ 's can be taken to be ambient metric balls. This is why we call the circular coordinates *sparse*;  $h_\eta$  is computed using only  $L$ , but its domain of definition is an open subset of  $\mathbb{M}$  which, by construction, contains all of  $X$ .

**1.3. Organization.** We start in Section 2 with a few preliminaries on principal bundles, highlighting the main theorems needed in later parts of the paper. We assume familiarity with persistent cohomology (if not, see [16]), as well as the definition of Čech cohomology with coefficients in a presheaf (see for instance [14]). Section 3 is devoted to deriving the formulas which turn a 1-dimensional integer cohomology class into a circle-valued function. In Section 4 we describe how to make all this theory applicable to real data sets. We present several experiments in Section 5 with both real and synthetic data, and end in Section 6 with a few final remarks.

## 2. PRELIMINARIES

**2.1. Principal Bundles.** We present here a terse introduction to principal bundles, with the main results we will need later in the paper. In particular, the connection between principal bundles and Čech cohomology, which allows for explicit computations, and their classification theory via homotopy classes of maps to classifying spaces. The latter description will be used to generate our sparse circular coordinates. We refer the interested reader to [9] for a more thorough presentation.

Let  $B$  be a connected and paracompact<sup>1</sup> topological space with basepoint  $b_0 \in B$ .

**Definition 2.1.** A pair  $(p, E)$ , with  $E$  a topological space and  $p : E \rightarrow B$  a continuous map, is said to be a fiber bundle over  $B$  with fiber  $F = p^{-1}(b_0)$ , if:

- (1)  $p$  is surjective
- (2) Every point  $b \in B$  has an open neighborhood  $U \subset B$  and a homeomorphism  $\rho_U : U \times F \rightarrow p^{-1}(U)$ , called a local trivialization around  $b$ , so that  $p \circ \rho_U(b', e) = b'$  for every  $(b', e) \in U \times F$ .

The spaces  $E$  and  $B$  are called, respectively, the total and base space of the bundle, and  $p$  is called the projection map.

**Definition 2.2.** Let  $G$  be an abelian topological group whose operation we write additively. A fiber bundle  $p : E \rightarrow B$  is said to be a principal  $G$ -bundle if:

- (1) The total space  $E$  comes equipped with a fiberwise free right  $G$ -action. That is, a continuous map

$$\cdot : E \times G \rightarrow E$$

satisfying the right-action axioms, with  $p(e \cdot g) = p(e)$  for every pair  $(e, g) \in E \times G$ , and for which  $e \cdot g = e$  only if  $g$  is the identity of  $G$ .

- (2) The induced fiberwise  $G$ -action  $p^{-1}(b) \times G \rightarrow p^{-1}(b)$  is transitive for every  $b \in B$  in the base space.
- (3) The local trivializations  $\rho_U : U \times F \rightarrow p^{-1}(U)$  can be chosen to be  $G$ -equivariant: that is, so that  $\rho_U(b, e \cdot g) = \rho_U(b, e) \cdot g$ , for every  $(b, e, g) \in U \times F \times G$ .

Given a principal  $G$ -bundle  $p : E \rightarrow B$  and a system of local trivializations  $\{\rho_j : U_j \times F \rightarrow p^{-1}(U_j)\}_{j \in J}$ , we have that

$$\rho_k^{-1} \circ \rho_j : (U_j \cap U_k) \times F \rightarrow (U_j \cap U_k) \times F \quad (2)$$

is a  $G$ -equivariant homeomorphism whenever  $U_j \cap U_k \neq \emptyset$ . Since the  $G$ -action on  $E$  is fiberwise free and fiberwise transitive, then  $\rho_k^{-1} \circ \rho_j$  induces a well-defined continuous map

$$\rho_{jk} : U_j \cap U_k \rightarrow G \quad j, k \in J$$

defined by the equation

$$\rho_k^{-1} \circ \rho_j(b, e) = (b, e \cdot \rho_{jk}(b)) \quad , \quad \text{for all } (b, e) \in (U_j \cap U_k) \times F. \quad (3)$$

The  $\rho_{jk}$ 's are called the transition functions for the  $G$ -bundle  $(p, E)$  corresponding to the system of local trivializations  $\{\rho_j\}_{j \in J}$ . In fact, these transition functions define an element in a Čech cohomology group of  $B$ . Indeed, for each open set  $U \subset B$  let  $\mathbf{Maps}(U, G)$  denote the set of continuous maps from  $U$  to  $G$ . Since  $G$  is

<sup>1</sup> So that partitions of unity always exist

an abelian group, then so is  $\mathbf{Maps}(U, G)$ , and if  $V \subset U$  is another open set, then precomposing with the inclusion  $V \hookrightarrow U$  yields a restriction map

$$\iota_{U,V} : \mathbf{Maps}(U, G) \longrightarrow \mathbf{Maps}(V, G)$$

This defines a sheaf  $\mathcal{C}_G$  of abelian groups over  $B$ , with  $\mathcal{C}_G(U) := \mathbf{Maps}(U, G)$ , called the sheaf of  $G$ -valued continuous functions on  $B$ . It follows that the transition functions (2) define an element  $\rho = \{\rho_{jk}\} \in \check{C}^1(\mathcal{U}; \mathcal{C}_G)$  in the Čech 1-cochains of the cover  $\mathcal{U} = \{U_j\}_{j \in J}$  with coefficients in the sheaf  $\mathcal{C}_G$ . Moreover,

**Proposition 2.3.** *The transition functions  $\rho_{jk}$  satisfy the cocycle condition*

$$\rho_{j\ell}(b) = (\rho_{jk} + \rho_{k\ell})(b) \quad \text{for all } b \in U_j \cap U_k \cap U_\ell \quad (4)$$

In other words,  $\rho = \{\rho_{jk}\} \in \check{Z}^1(\mathcal{U}; \mathcal{C}_G)$  is a Čech cocycle.

If  $\{\nu_r : V_r \times F \longrightarrow p^{-1}(V_r)\}_{r \in R}$  is another system of local trivializations with induced Čech cocycle  $\nu = \{\nu_{rs}\} \in \check{Z}^1(\mathcal{V}; \mathcal{C}_G)$ , and

$$\mathcal{W} = \{U_j \cap V_r\}_{(j,r) \in J \times R}$$

then one can check that the difference  $\rho - \nu$  is a coboundary in  $\check{C}^1(\mathcal{W}; \mathcal{C}_G)$ . Since  $\mathcal{W}$  is a refinement for both  $\mathcal{V}$  and  $\mathcal{U}$ , it follows that the  $G$ -bundle  $p : E \longrightarrow B$  yields a well-defined element  $p_E \in \check{H}^1(B; \mathcal{C}_G)$ . Moreover, after passing to isomorphism classes of  $G$ -bundles we get that

**Lemma 2.4.** *The function*

$$\begin{array}{ccc} \mathrm{Prin}_G(B) & \longrightarrow & \check{H}^1(B; \mathcal{C}_G) \\ [(p, E)] & \mapsto & p_E \end{array}$$

is well-defined and injective.

This is in fact a bijection. To check surjectivity, fix an open cover  $\mathcal{U} = \{U_j\}_{j \in J}$  for  $B$ , and a Čech cocycle

$$\eta = \{\eta_{jk}\} \in \check{Z}^1(\mathcal{U}; \mathcal{C}_G)$$

Then one can construct a  $G$ -principal bundle over  $B$  with total space

$$E_\eta = \left( \bigcup_{j \in J} U_j \times \{j\} \times G \right) / (b, j, g) \sim (b, k, g + \eta_{jk}(b)) \quad , \quad b \in U_j \cap U_k \quad (5)$$

and projection

$$p_\eta : E_\eta \longrightarrow B$$

taking the class of  $(b, j, g) \in U_j \times \{j\} \times G$  in the quotient  $E_\eta$ , to the point  $b \in B$ . Notice that if  $\eta_j : U_j \times G \longrightarrow E_\eta$  sends  $(b, g)$  to the class of  $(b, j, g)$  in  $E_\eta$ , then  $\{\eta_j\}$  defines a system of local trivializations for  $(p_\eta, E_\eta)$ , and that  $\eta = \{\eta_{jk}\}$  is the associated system of transition functions. Therefore,

**Theorem 2.5.** *The function*

$$\begin{array}{ccc} \check{H}^1(B; \mathcal{C}_G) & \longrightarrow & \mathrm{Prin}_G(B) \\ [\eta] & \mapsto & [E_\eta] \end{array}$$

is a natural bijection.

In addition to this characterization of principal  $G$ -bundles over  $B$  as Čech cohomology classes, there is another interpretation in terms of classifying maps. We will combine these two views in order to produce coordinates for data in the next sections.

To each topological group  $G$  one can associate a space  $EG$  that is both weakly contractible, i.e. all its homotopy groups are trivial, and which can be equipped with a free  $G$ -action

$$EG \times G \longrightarrow EG$$

For instance, one can take  $EG$  to be the Milnor construction [13]

$$EG := G * G * G * \cdots \quad (6)$$

with  $G$  acting diagonally by right multiplication on each term of the infinite join. The quotient  $BG := EG/G$  is a topological space (endowed with the quotient topology), called the classifying space of  $G$ , and the quotient map

$$j : EG \longrightarrow BG = EG/G$$

defines a principal  $G$ -bundle over  $BG$ , called the universal bundle. The next Theorem explains what universality means in this context.

Given a continuous map  $f : B \longrightarrow BG$ , the pullback  $f^*EG$  is a principal  $G$ -bundle over  $B$ , with total space  $\{(b, e) \in B \times EG : f(b) = j(e)\}$ , and projection map  $(b, e) \mapsto b$ . Moreover,

**Theorem 2.6.** *Let  $[B, BG]$  denote the set of homotopy class of maps from  $B$  to the classifying space  $BG$ . Then, the function*

$$\begin{array}{ccc} [B, BG] & \longrightarrow & \text{Prin}_G(B) \\ [f] & \mapsto & [f^*EG] \end{array}$$

*is a bijection.*

The previous theorem implies that given a principal  $G$ -bundle  $p : E \longrightarrow B$ , there exists a continuous map  $f : B \longrightarrow BG$  so that  $f^*EG$  is isomorphic to  $(p, E)$ , and that the choice of  $f$  is unique up to homotopy. Any such choice is called a classifying map for  $p : E \longrightarrow B$ .

### 3. FROM INTEGER SIMPLICIAL COHOMOLOGY TO CIRCULAR COORDINATES

For an arbitrary topological group  $G$ , the Milnor construction (6) produces an explicit universal  $G$ -bundle  $j : EG \longrightarrow BG$ , but the spaces  $EG$  and  $BG$  tend to be fairly large. Indeed, they are often infinite-dimensional CW-complexes. For the case  $G = \mathbb{Z}$  we have the more economical models  $E\mathbb{Z} \simeq \mathbb{R}$  and  $B\mathbb{Z} \simeq S^1 \subset \mathbb{C}$ , with  $\mathbb{Z}$  acting on  $\mathbb{R}$  by right translation:  $\mathbb{R} \times \mathbb{Z} \ni (r, m) \mapsto r + m$ , and projection

$$\begin{array}{ccc} p : \mathbb{R} & \longrightarrow & S^1 \\ r & \mapsto & \exp(2\pi ir) \end{array}$$

Since  $\mathbb{Z}$  is discrete, then  $\mathbb{Z}$ -valued continuous functions on  $B$  are in fact locally constant, and hence  $\mathcal{C}_{\mathbb{Z}}$  is exactly the sheaf of locally constant functions with values in  $\mathbb{Z}$ , denoted  $\underline{\mathbb{Z}}$ . Combining the definition of the Čech cohomology group  $\check{H}^1(B; \underline{\mathbb{Z}})$  with Theorems 2.5 and 2.6, yields a bijection

$$\varprojlim_{\mathcal{U}} H^1(\mathcal{N}(\mathcal{U}); \mathbb{Z}) \cong [B, S^1] \quad (7)$$

where the limit is taken over all covers  $\mathcal{U}$  of  $B$ , ordered by refinement, and the groups are the 1-dimensional simplicial cohomology with  $\mathbb{Z}$  coefficients of the associated nerve complexes  $\mathcal{N}(\mathcal{U})$ . The goal now is to produce an explicit family of compatible functions  $H^1(\mathcal{N}(\mathcal{U}); \mathbb{Z}) \rightarrow [B, S^1]$  realizing the isomorphism from (7). This is done in Theorem 3.3, and an explicit formula is given by (9) and then (11).

To begin, let  $\{\varphi_j\}_{j \in J}$  be a partition of unity on  $B$  dominated<sup>2</sup> by  $\mathcal{U} = \{U_j\}_{j \in J}$ , fix a 1-cocycle  $\eta = \{\eta_{jk}\} \in Z^1(\mathcal{N}(\mathcal{U}); \mathbb{Z})$ , and define for each  $j \in J$  the map

$$\begin{aligned} f_j : U_j \times \{j\} \times \mathbb{Z} &\longrightarrow \mathbb{R} \\ (b, j, n) &\longmapsto n + \sum_{\ell} \varphi_{\ell}(b) \eta_{j\ell} \end{aligned} \quad (8)$$

Note that  $\mathbb{Z}$  acts on  $U_j \times \{j\} \times \mathbb{Z}$  by right translation  $((b, j, n), m) \mapsto (b, j, n + m)$ , and that  $f_j$  is equivariant with respect to this action:  $f_j(b, j, n + m) = f_j(b, j, n) + m$ . Moreover, it follows directly from the definition that:

**Proposition 3.1.** *For all  $j \in J$ , the map  $f_j$  defined by (8) is injective on each orbit  $\{(b, j, n) : n \in \mathbb{Z}\}$ .*

If  $b \in U_j \cap U_k$ , then we have that

$$\begin{aligned} f_k(b, k, n + \eta_{jk}) &= n + \sum_{\ell \in J} \varphi_{\ell}(b) (\eta_{k\ell} + \eta_{jk}) \\ &= n + \sum_{\ell \in J} \varphi_{\ell}(b) \eta_{j\ell} \\ &= f_j(b, j, n) \end{aligned}$$

and hence the  $f_j$ 's can be assembled to induce a continuous map  $\tilde{f}_{\eta} : E_{\eta} \rightarrow \mathbb{R}$  on the quotient space defined by (5), where  $\eta = \{\eta_{jk}\} \in Z^1(\mathcal{N}(\mathcal{U}); \mathbb{Z})$  is regarded as a collection of constant functions  $\eta_{jk} : U_j \cap U_k \rightarrow \mathbb{Z}$ . To be more explicit,  $\tilde{f}_{\eta}$  sends the class of  $(b, j, n)$  in  $E_{\eta}$  to  $f_j(b, j, n) \in \mathbb{R}$ . Since each  $f_j$  is  $\mathbb{Z}$ -equivariant, then so is  $\tilde{f}_{\eta}$ , and hence it descends to a map at the level of base spaces

$$\begin{aligned} f_{\eta} : B &\longrightarrow S^1 \subset \mathbb{C} \\ U_j \ni b &\longmapsto \exp \left( 2\pi i \sum_k \varphi_k(b) \eta_{jk} \right) \end{aligned} \quad (9)$$

**Proposition 3.2.** *The map  $f_{\eta}$  classifies the  $\mathbb{Z}$ -principal bundle  $E_{\eta}$ .*

*Proof.* It is enough to show that  $\tilde{f}_{\eta} : E_{\eta} \rightarrow \mathbb{R}$  is a homeomorphism on each orbit. Since each  $f_j$  is a bijection when restricted to the orbit of a point  $(b, j, n)$ , the result follows.  $\square$

**Theorem 3.3.** *Let  $\iota : \mathbb{Z} \hookrightarrow \mathbb{R}$  be the inclusion and*

$$\iota^* : H^1(\mathcal{N}(\mathcal{U}); \mathbb{Z}) \longrightarrow H^1(\mathcal{N}(\mathcal{U}); \mathbb{R}) \quad (10)$$

*the induced homomorphism. Given  $\eta \in Z^1(\mathcal{N}(\mathcal{U}); \mathbb{Z})$ , let  $\theta \in Z^1(\mathcal{N}(\mathcal{U}); \mathbb{R})$  be a representative for  $\iota^*([\eta])$ , and let  $\tau \in C^0(\mathcal{N}(\mathcal{U}); \mathbb{R})$  be so that  $\iota^{\#}(\eta) = \theta - \delta^0 \tau$ . If*

$$\begin{aligned} h_{\theta, \tau} : B &\longrightarrow S^1 \subset \mathbb{C} \\ U_j \ni b &\longmapsto \exp \left\{ 2\pi i \left( \tau_j + \sum_k \varphi_k(b) \theta_{jk} \right) \right\} \end{aligned} \quad (11)$$

*then  $h_{\theta, \tau}$  is a classifying map for the  $\mathbb{Z}$ -principal bundle  $E_{\eta}$ .*

<sup>2</sup> That is, so that  $\text{support}(\varphi_j) \subset \text{closure}(U_j)$  for all  $j \in J$ .

*Proof.* For  $b \in U_j$  we have that

$$\begin{aligned}
 f_\eta(b) &= \exp \left( 2\pi i \sum_k \varphi_k(b) \eta_{jk} \right) \\
 &= \exp \left( 2\pi i \sum_k \varphi_k(b) (\theta_{jk} + \tau_j - \tau_k) \right) \\
 &= \exp \left( 2\pi i \left( \tau_j + \sum_k \varphi_k(b) (\theta_{jk} - \tau_k) \right) \right) \\
 &= \nu_\tau(b) \cdot h_{\theta, \tau}(b)
 \end{aligned}$$

where  $\nu_\tau(b) = \exp \left( -2\pi i \sum_k \varphi_k(b) \tau_k \right)$ . Since  $\nu_\tau$  factors through  $\mathbb{R}$ :

$$\begin{array}{ccccc}
 \nu_\tau : B & \longrightarrow & \mathbb{R} & \longrightarrow & S^1 \subset \mathbb{C} \\
 b & \mapsto & \sum_k \varphi_k(b) \tau_k & \mapsto & \exp \left( -2\pi i \sum_k \varphi_k(b) \tau_k \right)
 \end{array}$$

then it is null-homotopic, hence  $f_\eta$  is homotopic to  $h_{\theta, \tau}$ , and the result follows.  $\square$

#### 4. PERSISTENT COHOMOLOGY AND SPARSE CIRCULAR COORDINATES FOR DATA

In this section we show how the theory we have developed thus far can be applied to real data sets. In particular, we explain and justify the choices made in the construction outlined in the Introduction (1.2). Let us begin by fixing an ambient metric space  $(\mathbb{M}, \mathbf{d})$ , let  $L \subset \mathbb{M}$  be finite, and let

$$\begin{aligned}
 B_\alpha(\ell) &= \{b \in \mathbb{M} : \mathbf{d}(b, \ell) < \alpha\} \quad , \quad \alpha \geq 0, \ell \in L \\
 \mathcal{B}_\alpha &= \{B_\alpha(\ell)\}_{\ell \in L} \\
 L^{(\alpha)} &= \bigcup \mathcal{B}_\alpha
 \end{aligned}$$

The formulas derived in the previous section, specially (9), imply that each cocycle  $\eta \in Z^1(\mathcal{N}(\mathcal{B}_\alpha); \mathbb{Z})$  yields a map  $h : L^{(\alpha)} \rightarrow S^1$ . The thing to notice is that  $h$  is defined on every  $x \in L^{(\alpha)}$ ; thus, given a large but finite set  $X \subset \mathbb{M}$  — the data — sampled around a continuous space  $\mathbb{X} \subset \mathbb{M}$ , one can select a much smaller set of landmarks  $L \subset X$  and  $\alpha > 0$  for which  $X \subset L^{(\alpha)}$ . The resulting circular coordinates  $h : L^{(\alpha)} \rightarrow S^1$  will thus be defined on all points of  $X$ , though only the landmark set is used in its construction. As we alluded to in the introduction, this is what we mean when we say that the coordinates are *sparse*.

**Landmark Selection.** In practice we select the landmarks  $L \subset X$  either at random, or through **maxmin** sampling: Given  $N \leq |X|$  and  $\ell_1 \in X$  chosen arbitrarily, assume that  $\ell_1, \dots, \ell_j \in X$  have been selected,  $1 \leq j < N$ , and let

$$\ell_{j+1} = \operatorname{argmax}_{x \in X} \min \{ \mathbf{d}(x, \ell_1), \dots, \mathbf{d}(x, \ell_j) \} \quad (12)$$

Following this inductive procedure defines a landmark set  $L = \{\ell_1, \dots, \ell_N\} \subset X$  that is in practice well-separated and well-distributed throughout the data. However, it is important to keep in mind that this process is prone to choosing outliers.



**The Subordinated Partition of Unity.** As for the choice of partition of unity  $\{\varphi_\ell\}_{\ell \in L}$  dominated by  $\mathcal{B}_\alpha$ , we can use that the cover is via metric balls, and let

$$\varphi_\ell(b) = \frac{|\alpha - \mathbf{d}(\ell, b)|_+}{\sum_{\ell' \in L} |\alpha - \mathbf{d}(\ell', b)|_+} \quad \text{where} \quad |r|_+ = \max\{r, 0\}, \quad r \in \mathbb{R} \quad (13)$$

See [17, 3.3 and Fig 6.] for other typical choices of partition of unity in the case of metric spaces, and coverings via metric balls.

**The Need for Persistence.** Even if the landmark set  $L$  correctly approximates the underlying topology of  $X$ , the choice of scale  $\alpha > 0$  and cocycle  $\eta \in Z^1(\mathcal{N}(\mathcal{B}_\alpha); \mathbb{Z})$  might reflect sampling artifacts instead of robust geometric features of the underlying space  $\mathbb{X}$ . This is why we need persistent cohomology. Indeed, a class  $[\eta] \in H^1(\mathcal{N}(\mathcal{B}_\alpha); \mathbb{Z})$  which is not in the kernel of the homomorphism

$$H^1(\mathcal{N}(\mathcal{B}_\alpha); \mathbb{Z}) \longrightarrow H^1(\mathcal{N}(\mathcal{B}_{\alpha'}); \mathbb{Z}) \quad , \quad 0 < \alpha' < \alpha$$

induced by the inclusion  $\mathcal{N}(\mathcal{B}_{\alpha'}) \subset \mathcal{N}(\mathcal{B}_\alpha)$ , is less likely to correspond to spurious features as the difference  $\alpha - \alpha'$  increases. Note, however, that the efficient computation of persistent cohomology classes relies on using field coefficients. We proceed, following [6] and [17], by choosing a prime  $q$  and a scale  $\alpha > 0$  so that (1)  $H^1(\mathcal{N}(\mathcal{B}_\alpha); \mathbb{Z}/q)$  contains a class with large persistence, and (2) so that the homomorphism  $H^1(\mathcal{N}(\mathcal{B}_\alpha); \mathbb{Z}) \longrightarrow H^1(\mathcal{N}(\mathcal{B}_\alpha); \mathbb{Z}/q)$ , induced by the quotient map  $\mathbb{Z} \longrightarrow \mathbb{Z}/q$ , is surjective.

**Lifting Persistence to Integer Coefficients.** As stated in [6], one has that:

**Proposition 4.1.** *Let  $K$  be a finite simplicial complex, and suppose that  $q \in \mathbb{N}$  does not divide the order of the torsion subgroup of  $H^2(K; \mathbb{Z})$ . Then the homomorphism*

$$\iota_q^* : H^1(K; \mathbb{Z}) \longrightarrow H^1(K; \mathbb{Z}/q)$$

*induced by the quotient map  $\iota_q : \mathbb{Z} \longrightarrow \mathbb{Z}/q$ , is surjective.*

*Proof.* This follows directly from the Bockstein long exact sequence in cohomology, corresponding to the short exact sequence  $0 \longrightarrow \mathbb{Z} \xrightarrow{\times q} \mathbb{Z} \xrightarrow{\iota_q} \mathbb{Z}/q \longrightarrow 0$ .  $\square$

More generally, let  $\{K_\alpha\}_{\alpha \geq 0}$  be a filtered simplicial complex with  $\bigcup_{\alpha \geq 0} K_\alpha$  finite.

Since each complex  $K_\alpha$  is finite, and the cohomology groups  $H^2(K_\alpha; \mathbb{Z})$  change only at finitely many values of  $\alpha$ , then there exists  $Q \in \mathbb{N}$  so that the hypotheses of Proposition 4.1 will be satisfied for each  $q \geq Q$ , and all  $\alpha \geq 0$ . In practice we choose a prime  $q$  at random, with the intuition that for scientific data only a few primes are torsion contributors.

Let  $\mathbb{Z}/q = \{0, 1, \dots, q-1\}$  and for  $\eta' \in Z^1(K_\alpha; \mathbb{Z}/q)$  let  $\eta \in C^1(K_\alpha; \mathbb{Z})$  be defined on each 1-simplex  $\sigma \in K_\alpha$  as:

$$\eta(\sigma) = \begin{cases} \eta'(\sigma) & \text{if } \eta'(\sigma) \leq \frac{q-1}{2} \\ \eta'(\sigma) - q & \text{if } \eta'(\sigma) > \frac{q-1}{2} \end{cases} \quad (14)$$

Thus,  $\eta$  takes values in  $\{-\frac{q-1}{2}, \dots, 0, \dots, \frac{q-1}{2}\} \subset \mathbb{Z}$  and it satisfies  $(\eta \bmod q) = \eta'$ . For all examples we have observed, the cochain defined by (14) produces an integer cocycle. However, as highlighted in [6, 2.4], this is not guaranteed and in case of failure one has to solve a Diophantine linear system to fix the problem.

**Use Rips, not Nerves.** Constructing the filtered complex  $\{\mathcal{N}(\mathcal{B}_\alpha)\}_{\alpha \geq 0}$  can be rather expensive for a general ambient metric space  $(\mathbb{M}, \mathbf{d})$ . Indeed, the inclusion of an  $n$ -simplex into the nerve complex is predicated on checking if the intersection of  $n + 1$  ambient metric balls is nonempty. This is nontrivial on curved spaces. On the other hand, the Rips complex

$$R_\alpha(L) = \{\sigma \subset L : \text{diam}(\sigma) < \alpha\} \quad , \quad \alpha \geq 0$$

provides a straightforward alternative, since we can use that

$$R_\alpha(L) \subset \mathcal{N}(\mathcal{B}_\alpha) \subset R_{2\alpha}(L)$$

for every  $\alpha \geq 0$ . Here is how. Let  $q > 2$  be a prime so that

$$\iota_q^* : H^1(R_\alpha(L); \mathbb{Z}) \longrightarrow H^1(R_\alpha(L); \mathbb{Z}/q)$$

is surjective for all  $\alpha \geq 0$ , and let

$$j : H^1(R_{2\alpha}(L); \mathbb{Z}/q) \longrightarrow H^1(R_\alpha(L); \mathbb{Z}/q)$$

be the homomorphism induced by the inclusion  $R_\alpha(L) \subset R_{2\alpha}(L)$ . Moreover, let  $\eta' \in Z^1(R_{2\alpha}(L); \mathbb{Z}/q)$  be so that  $[\eta'] \notin \text{Ker}(j)$ , and fix an integer lift

$$\eta \in Z^1(R_{2\alpha}(L); \mathbb{Z})$$

That is, one for which  $\eta' - (\eta \bmod q) \in Z^1(R_{2\alpha}(L); \mathbb{Z})$  is a coboundary, e.g. (14).

The diagram below summarizes the spaces and homomorphisms used thus far:

$$\begin{array}{ccccc} [\eta'] \in H^1(R_{2\alpha}(L); \mathbb{Z}/q) & \xleftarrow{\iota_q^*} & H^1(R_{2\alpha}(L); \mathbb{Z}) \ni [\eta] & & \\ & \downarrow & \downarrow \iota_{\mathbb{Z}}^* & & \\ j \left( \begin{array}{ccc} H^1(\mathcal{N}(\mathcal{B}_\alpha); \mathbb{Z}/q) & \xleftarrow{\iota_q^*} & H^1(\mathcal{N}(\mathcal{B}_\alpha); \mathbb{Z}) \ni [\tilde{\eta}] \\ \downarrow & & \\ H^1(R_\alpha(L); \mathbb{Z}/q) & & \end{array} \right. & & & & \end{array}$$

Since the diagram commutes, then  $[\eta]$  is not in the kernel of  $\iota_{\mathbb{Z}}^*$ , and hence we obtain a nonzero element  $\iota_{\mathbb{Z}}^*([\eta]) = [\tilde{\eta}] \in H^1(\mathcal{N}(\mathcal{B}_\alpha); \mathbb{Z})$ . This is the class we would use as input for Theorem 3.3.

**Harmonic Smoothing.** The final step is selecting an appropriate cocycle representative (refer to Figure 1 to see why this matters)

$$\tilde{\theta} \in Z^1(\mathcal{N}(\mathcal{B}_\alpha); \mathbb{R})$$

for the class  $\iota^*([\tilde{\eta}]) \in H^1(\mathcal{N}(\mathcal{B}_\alpha); \mathbb{R})$ , see (10). Again, since one would hope to never compute the nerve complex, the strategy is to solve the problem in  $Z^1(R_{2\alpha}(L); \mathbb{R})$  for  $\iota^\#(\eta)$ , and then transfer the solution using  $\iota_{\mathbb{R}}^\# : C^1(R_{2\alpha}(L); \mathbb{R}) \rightarrow C^1(\mathcal{N}(\mathcal{B}_\alpha); \mathbb{R})$ .

Inspecting (11) reveals that the choice of  $\tilde{\theta}$  which promotes the smallest total variation in  $h_{\tilde{\theta}, \tilde{\tau}}$ , is the one for which the value of  $\tilde{\theta}$  on each 1-simplex of  $\mathcal{N}(\mathcal{B}_\alpha)$  is as small as possible. Consequently, we will look for the cocycle representative

$$\theta \in Z^1(R_{2\alpha}(L); \mathbb{R})$$

of  $\iota^*([\eta])$ , which in average has the smallest squared value<sup>3</sup> on each 1-simplex of  $R_{2\alpha}(L)$ . That said, not all edges in the rips complex  $R_\epsilon(L)$  are created equal.

<sup>3</sup> That is, we use the harmonic cocycle representative for appropriate inner products on cochains

Some might have just entered the filtration, i.e.  $\mathbf{d}(\ell_j, \ell_k) \approx \epsilon$ , which would make them unstable if  $L$  is corrupted with noise, or perhaps  $X \cap (B_{\epsilon/2}(\ell_j) \cup B_{\epsilon/2}(\ell_k))$  is a rather small portion of the data, which could happen if  $\ell_j$  and  $\ell_k$  are outliers selected during **maxmin** sampling.

These observations can be encoded by choosing weights on vertices and edges defined via a one-parameter family of symmetric functions

$$\omega_\epsilon : L \times L \longrightarrow [0, \infty) \quad , \quad \epsilon \geq 0 \quad (15)$$

so that

$$\omega_{\epsilon'}(\ell, \ell') \leq \omega_\epsilon(\ell, \ell') \quad , \quad \text{for } \epsilon' \leq \epsilon$$

and for which  $\omega_\epsilon(\ell, \ell') = 0$  only when  $0 < \epsilon \leq \mathbf{d}(\ell, \ell')$ . Here  $\omega_\epsilon(\ell, \ell)$  is the weight of  $\ell$ , and  $\omega_\epsilon(\ell, \ell')$  is the weight of the edge  $\{\ell, \ell'\}$ . For instance, one can take

$$\omega_\epsilon(\ell, \ell') = |\epsilon - \mathbf{d}(\ell, \ell')|_+$$

but we note that we have not yet systematically investigated the effects of this choice. See [20, Appendix D] for a different heuristic.

It follows that  $\omega_\epsilon$  defines inner products  $\langle \cdot, \cdot \rangle_\epsilon$  on  $C^0(R_\epsilon(L); \mathbb{R})$  and  $C^1(R_\epsilon(L); \mathbb{R})$ , by letting the indicator functions  $1_\sigma$  on  $k$ -simplices ( $k = 0, 1$ )  $\sigma \in R_\epsilon(L)$  be orthogonal, and setting

$$\langle 1_\sigma, 1_\sigma \rangle_\epsilon = \omega_\epsilon(\sigma) \quad (16)$$

Using  $\langle \cdot, \cdot \rangle_\epsilon$ , for  $\epsilon = 2\alpha$ , we let  $\beta \in B^1(R_{2\alpha}(L); \mathbb{R})$  be the orthogonal projection of  $\iota^\#(\eta)$  onto the space of 1-coboundaries, and define

$$\theta = \iota^\#(\eta) - \beta \quad (17)$$

A bit of linear algebra shows that,

**Proposition 4.2.** *The 1-cocycle  $\theta$  defined by (17) is a minimizer for the weighted least squares problem*

$$\min_{\phi \sim \iota^\#(\eta)} \sum_{\sigma} \omega_{2\alpha}(\sigma) \cdot \phi(\sigma)^2 \quad (18)$$

Here the sum runs over all 1-simplices  $\sigma \in R_{2\alpha}(L)$ , and the minimization is over all 1-cocycles  $\phi \in Z^1(R_{2\alpha}(L); \mathbb{R})$  which are cohomologous to  $\iota^\#(\eta)$ .

Similarly, and if

$$d_{2\alpha} : C^0(R_{2\alpha}(L); \mathbb{R}) \longrightarrow C^1(R_{2\alpha}(L); \mathbb{R})$$

denotes the coboundary map, then we let

$$\tau \in \text{Ker}(d_{2\alpha})^\perp \subset C^0(R_{2\alpha}(L); \mathbb{R})$$

in the orthogonal complement of the kernel of  $d_{2\alpha}$ , be so that  $d_{2\alpha}(\tau) = -\beta$ . Hence  $\tau$  is the 0-chain with the smallest norm mapping to  $-\beta$  via  $d_{2\alpha}$ . Consequently, if

$$d_{2\alpha}^+ : C^1(R_{2\alpha}(L); \mathbb{R}) \longrightarrow C^0(R_{2\alpha}(L); \mathbb{R})$$

is the weighted Moore-Penrose pseudoinverse of  $d_{2\alpha}$  (see [3, III.3.4]), then

$$\tau = -d_{2\alpha}^+(\iota^\#(\eta)) \quad \text{and} \quad \theta = \iota^\#(\eta) + d_{2\alpha}(\tau) \quad (19)$$

This is how we compute  $\tau$  and  $\theta$  in our implementation. Now, let

$$\tilde{\tau} = \iota_{\mathbb{R}}^\#(\tau) \in C^0(\mathcal{N}(\mathcal{B}_\alpha); \mathbb{R})$$

$$\tilde{\theta} = \iota_{\mathbb{R}}^\#(\theta) \in Z^1(\mathcal{N}(\mathcal{B}_\alpha); \mathbb{R})$$

If we were to be completely rigorous, then  $\tilde{\tau}$  and  $\tilde{\theta}$  would be the cochains going into (11); this would require the 1-skeleton of the nerve complex. However, as the following proposition shows, this is unnecessary:

**Proposition 4.3.** *For all  $b \in B_\alpha(\ell_j)$ , and every  $j = 1, \dots, N$ , we have that*

$$\exp \left\{ 2\pi i \left( \tilde{\tau}_j + \sum_{k=1}^N \varphi_k(b) \tilde{\theta}_{jk} \right) \right\} = \exp \left\{ 2\pi i \left( \tau_j + \sum_{k=1}^N \varphi_k(b) \theta_{jk} \right) \right\}$$

*That is, we can compute sparse circular coordinates using only the Rips complex on the landmark set.*

*Proof.* Since  $\mathcal{N}(\mathcal{B}_\alpha)$  and  $R_{2\alpha}(L)$  have the same vertex set, namely  $L$ , then  $\tilde{\tau} = \tau$  as real-valued functions on  $L$ . Moreover, for all  $k = 1, \dots, N$  we have that

$$\varphi_k(b) \tilde{\theta}_{jk} = \varphi_k(b) \theta_{jk}$$

for if  $b \notin B_\alpha(\ell_k)$ , then both sides are zero, and if  $b \in B_\alpha(\ell_j) \cap B_\alpha(\ell_k)$ , then the edge  $\{\ell_j, \ell_k\}$  is in both  $R_{2\alpha}(L)$  and  $\mathcal{N}(\mathcal{B}_\alpha)$ , which shows that  $\tilde{\theta}_{jk} = \theta_{jk}$ .  $\square$

## 5. EXPERIMENTS

In all experiments below, persistent cohomology is computed using a MATLAB wrapper for Ripser [1] kindly provided by [Chris Tralie](#). The Moore-Penrose pseudoinverse was computed via MATLAB's `pinv`. In all cases we run the algorithm from the Introduction 1.2 using the indicated persistence classes, or linear combinations thereof as made explicit in each example.

### 5.1. Synthetic Data.

**5.1.1. A Noisy Circle.** We select 1,000 points from a noisy circle in  $\mathbb{R}^2$ ; the noise is Gaussian in the direction normal to the unit circle. 50 landmarks were selected via `maxmin` sampling (5% of the data), and circular coordinates were computed for the two most persistent classes  $\eta_1$  and  $\eta_2$ , using (19) as input to (11) — this is the harmonic cocycle column — or (9) with either  $\eta_1$  or  $\eta_2$  directly — the integer cocycle column. We show the results in Figure 1 below. Computing persistent cohomology took 0.079423 seconds (the Rips filtration is constructed from zero to the diameter of the landmark set); in each case computing the harmonic cocycle takes about 0.037294 seconds. This example highlights the inadequacy of the integer cocycle and of choosing cohomology classes associated to sampling artifacts (i.e., with low persistence). From now on, we only present circular coordinates computed with the relevant harmonic cocycle representative.

**5.1.2. The 2-Dimensional Torus.** For this experiment we sample 1,000 points uniformly at random from the square  $[0, 2\pi) \times [0, 2\pi)$ , and for each selected pair  $(\phi_1, \phi_2)$  we generate a point  $(e^{i\phi_1}, e^{i\phi_2}) \in S^1 \times S^1$  on the surface of the torus embedded in  $\mathbb{C}^2$ . The resulting finite set is endowed with the ambient distance from  $\mathbb{C}^2$ , and 100 landmarks (i.e., 10% of the data) are selected through `maxmin` sampling. We show the results in Figure 2 below, for the circular coordinates computed with the two most persistent classes,  $\eta_1$  and  $\eta_2$ , and the maps (11) associated to the harmonic cocycle representatives (19). Computing persistent cohomology for the Rips filtration on the Landmarks (from zero to the diameter of the set) takes 0.398252 seconds, and computing the harmonic cocycles takes about 0.030832 seconds.

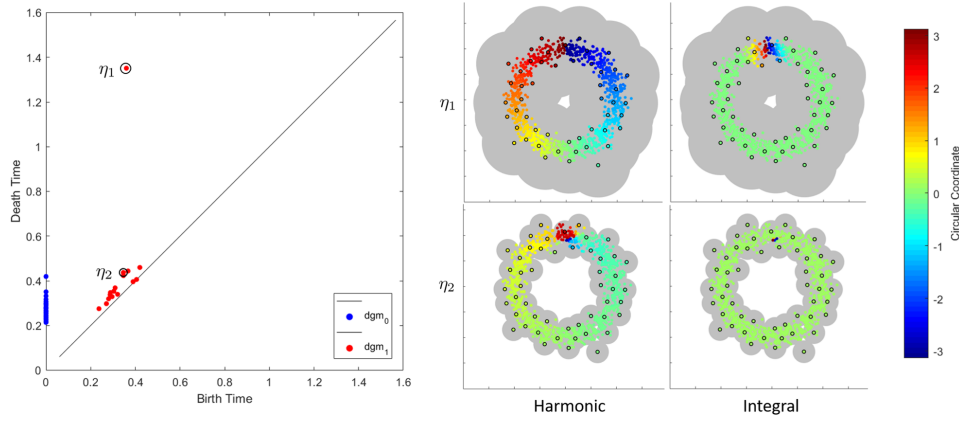


FIGURE 1. A noisy circle. Left: persistence diagrams in dimension 0 (blue) and 1 (red) for the Rips filtration on the landmarks. Right: Circular coordinates from the two most persistent classes  $\eta_1$  (top row) and  $\eta_2$  (bottom row). The columns indicate if the harmonic or integral cocycle was used. The dark rings are the landmarks. The colors are: the domain of definition for the circular coordinate (gray), and its value on each point (dark blue,  $-\pi$ , through dark red,  $\pi$ ). Please refer to an electronic version for colors.

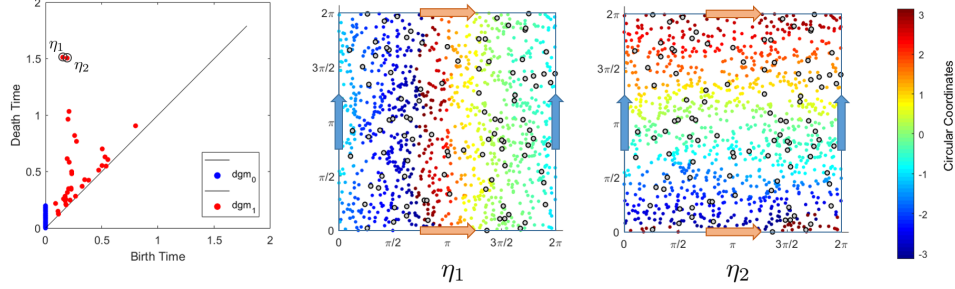


FIGURE 2. The torus. Left: Persistence in dimensions 0 and 1 for the Rips filtration on the landmark set. Center and Right: the landmark set is depicted with dark rings, and the colors correspond to the circular coordinates computed with (the harmonic representatives from) the two most persistent classes  $\eta_1$  (center) and  $\eta_2$  (right). The arrows in blue and orange indicate the identifications in the boundary of the square  $[0, 2\pi] \times [0, 2\pi]$  giving rise to the 2-torus. Please refer to an electronic version for colors.

5.1.3. *The Klein Bottle.* We model the Klein bottle as the quotient space

$$K = S^1 \times S^1 / (z, w) \sim (-z, \bar{w})$$

and endow it with the quotient metric. Just like in the case of the 2-torus, we sample 1,000 points uniformly at random on (the fundamental domain  $[0, \pi] \times [0, 2\pi]$  of)  $K$ , and select 100 landmarks via `maxmin` sampling and the quotient metric. Below

in Figure 3 we show the results of computing the persistent cohomology, with coefficients in  $\mathbb{Z}/13$ , of the Rips filtration on the landmark set (left), along with the circular coordinates corresponding to the most persistent class (right).

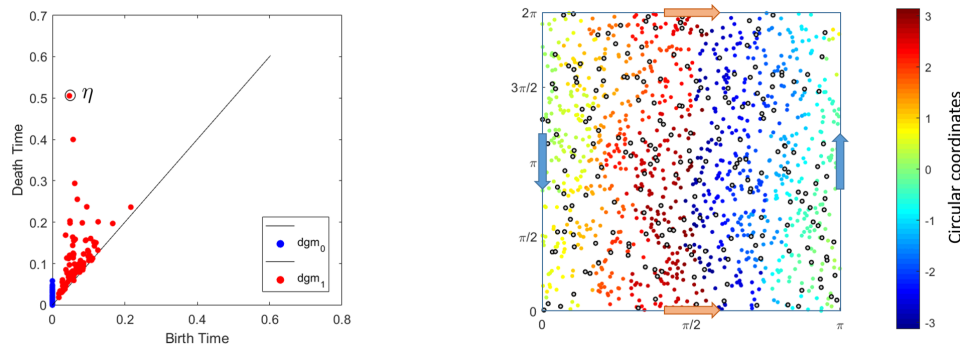


FIGURE 3. Circular coordinates on the Klein bottle. Left: Persistence with coefficients in  $\mathbb{Z}/13$  for the Rips filtration on the landmark set. Right: Circular coordinates computed from the harmonic representative from the class  $\eta$  with largest persistence. The arrows in blue and orange indicate the identifications on the boundary of  $[0, \pi] \times [0, 2\pi]$  giving rise to the Klein bottle. Dark rings indicate landmarks, and the colors (dark blue through dark red) are the angular values of the circular coordinate on each data point. Please refer to an electronic version for colors.

## 5.2. Real Data.

5.2.1. *COIL 20*. The Columbia University Image Library (COIL-20) is a collection of  $448 \times 416$ -pixel gray scale images from 20 objects, each of which is photographed at 72 different rotation angles [15]. The database has two versions: a processed version, where the images have been cropped to show only the rotated object, and an unprocessed version with the 72 raw images from 5 objects. We will analyze the unprocessed database, of which a few examples are shown in Figure 4 below.

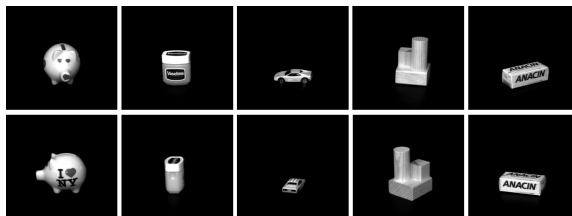


FIGURE 4. Some examples from the unprocessed COIL20 image database

Regarding each image as a vector of pixel intensities in  $\mathbb{R}^{448 \times 416}$  yields a set  $X$  with 360 points; this set becomes a finite metric space when endowed with the ambient Euclidean distance. Below in Figure 5 (left) we show the result of computing persistence (this time visualized as barcodes) for the Rips complex on

the entire data set (0.293412 seconds). Each one of the six most persistent classes  $\eta_1, \dots, \eta_6$  yields a circle-valued map on the data  $h_j : X \rightarrow S^1$ ,  $j = 1, \dots, 6$ . Multiplying these maps together, using the group structure from  $S^1 \subset \mathbb{C}$ , yields a map  $h : X \rightarrow S^1$ . We do this at the level of maps, as opposed to adding up the cocycle representatives, because there is no scale  $\alpha$  at which all these classes are alive. We also show in Figure 5 (right) an Isomap [22] projection of the data into  $\mathbb{R}^2$ , and we color each projected data point with its  $h$  value.

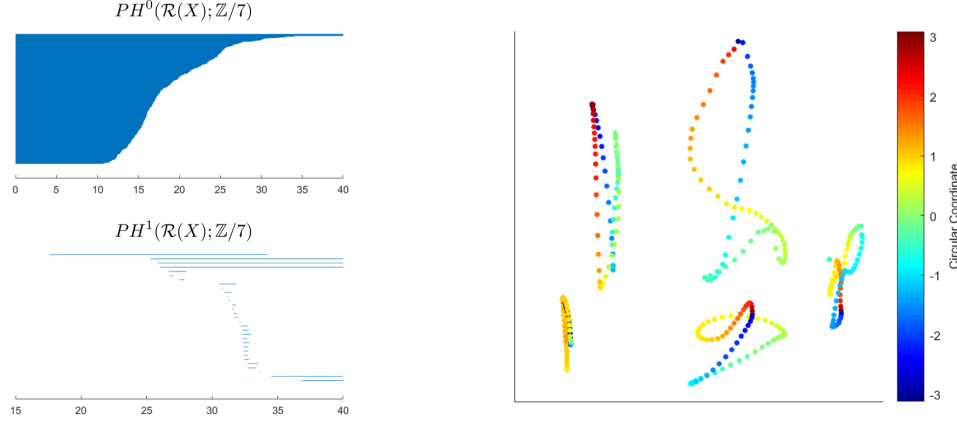


FIGURE 5. COIL-20 Unprocessed. Left: Persistence of the Rips filtration. Right: Isomap projection colored by circular coordinate.

As we show in Figure 6 below, a better system of coordinates for the data (i.e. one without crossings) is given by the computed circular coordinate of each data point, and the cluster (computed using single linkage) to which it belongs to.

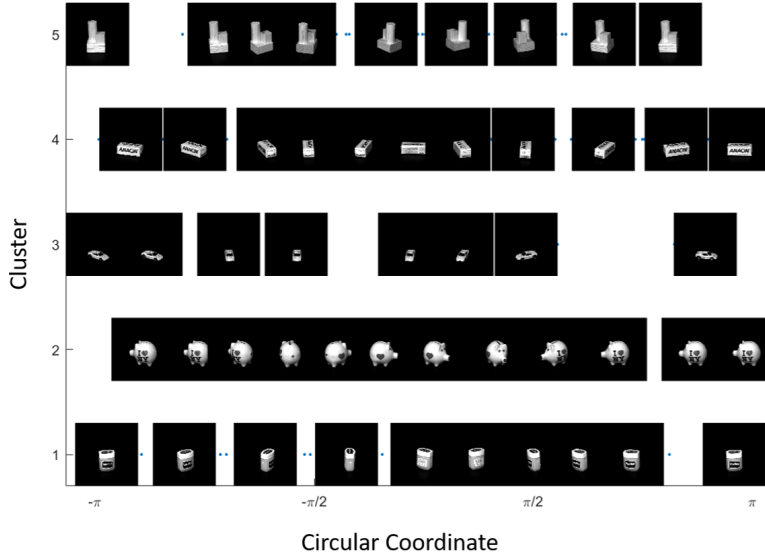


FIGURE 6. COIL-20 Unprocessed: Clusters vs Circular coordinates

**5.2.2. The Mumford Data.** This data set was first introduced in [12], with an initial exploration of its underlying topological structure done in [5], and then a more thorough investigation in [4]. The data set in question is a collection of roughly 4 million  $3 \times 3$ -pixel gray-scale images with high-contrast, selected from monochrome photos in a database of 4,000 natural scenes [8]. The  $3 \times 3$ -pixel image patches are preprocessed, intensity-centered and contrast-normalized, and a linear change of coordinates is performed yielding a point-cloud  $\mathcal{M} \subset S^7 \subset \mathbb{R}^8$ . The Euclidean distance in  $\mathbb{R}^8$  endows  $\mathcal{M}$  with the structure of a finite metric space. Following [4], we select 50,000 points at random from  $\mathcal{M}$  and then let  $X$  be the top 30% densest points as measured by the distance to their 15th nearest neighbor. This results in a data set with 15,000 points, which we analyze below.

We select 700 landmarks from  $X$  via `maxmin` sampling, i.e. 4.7% of  $X$ , and compute persistence for the associated Rips filtration. This takes about 2.2799 seconds and the result is shown in Figure 7 below.

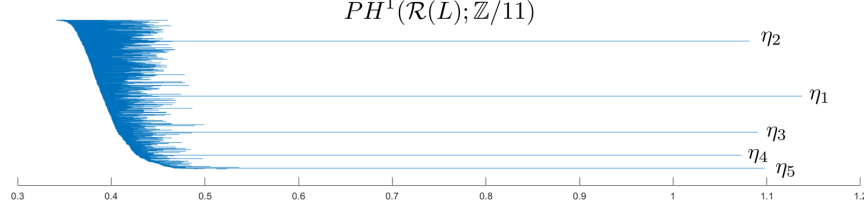


FIGURE 7. Barcodes from persistence on the Rips filtration of the landmark set  $L \subset X$ .

Each bar in the barcode yields a class  $\eta_j$ , which we order from largest ( $\eta_1$ ) to smallest ( $\eta_5$ ) persistence. Below in Figure 8 we show the circular coordinates associated to the classes  $\eta_2$ ,  $\eta_1 + \eta_5$  and  $\eta_3 + \eta_4$ , respectively. Each of the three panels shows a scatter plot of  $X \subset \mathbb{R}^8$  with respect to the first two coordinates, dark rings are the selected landmarks, and the colors (dark blue through dark red) are the circular coordinates corresponding to the indicated persistence classes. The computation of each cocycle representative takes about 7.1434 seconds, so the entire analysis is less than 25 seconds.

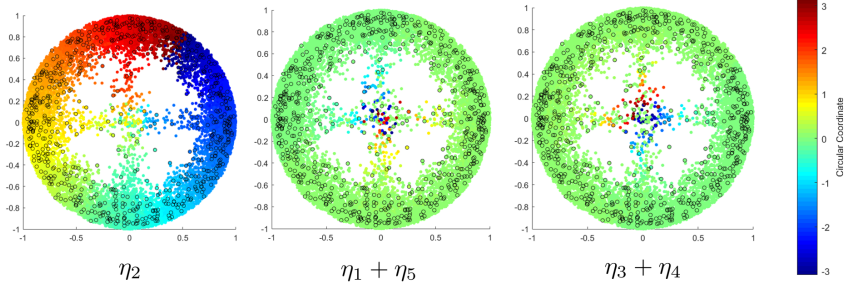


FIGURE 8. Circular coordinates for the points in  $X \subset \mathbb{R}^8$ , plotted according to their first two coordinates, and colored by the circular coordinates associated to each one of the classes  $\eta_2$  (left),  $\eta_1 + \eta_5$  (center) and  $\eta_3 + \eta_4$  (right).



These three circular coordinates allow us to map the data set  $X$  into the 3-dimensional torus  $T^3 = S^1 \times S^1 \times S^1$ , which we model as the 3-dimensional cube  $[-\pi, \pi] \times [-\pi, \pi] \times [-\pi, \pi]$  with opposite faces identified. We show in Figure 9 below the result of mapping the data into  $T^3$ .

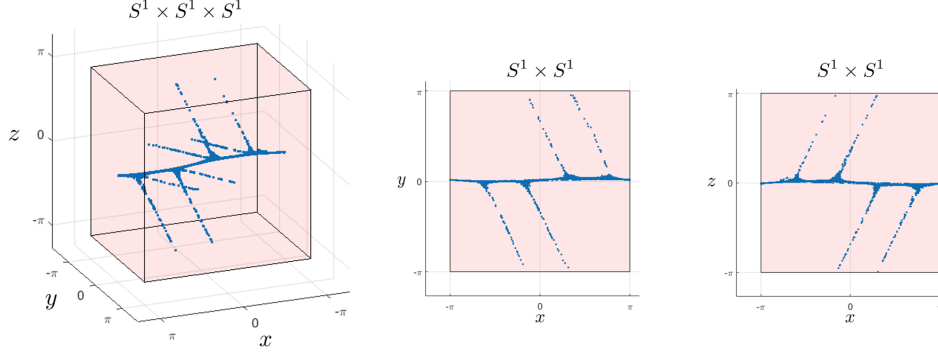


FIGURE 9. Scatter plot in the 3-torus (left) for  $X$ , along with two 2-d projections (center, right). The horizontal line on the  $xy$  plane is a circle (the primary circle), and each one of the four V-shaped curves in  $T^3$  is a hemisphere of a (secondary) circle.

As we can see from the scatter plot, these three coordinates provide a faithful realization of the data in the three circle model proposed in [4]. Below in Figure 10 we show some of these image patches in their  $T^3$ -coordinate to better illustrate what the actual circles are.

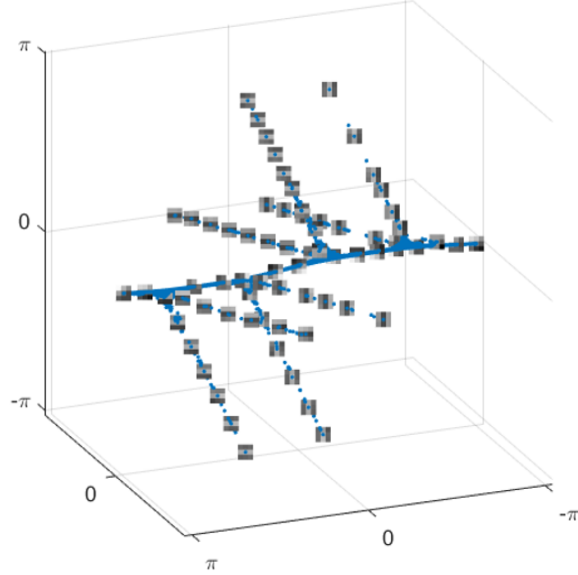


FIGURE 10. Image patches from  $X$ , plotted at their location in the 3-torus, according to the computed circular coordinates.

## 6. DISCUSSION

We have presented in this paper an application of the theory of principal bundles, to the problem of finding topologically and geometrically meaningful coordinates for scientific data. Specifically, we leverage the 1-dimensional persistent cohomology of the Rips filtration on a subset of the data (the landmarks), in order to produce  $S^1$ -valued coordinates on the entire data set. The coordinates are designed to capture 1-dimensional topological features of a continuous underlying space, and the theory on which the coordinates are built, indicates that they classify  $\mathbb{Z}$ -principal bundles on the continuum.

The use of bundle theory allows for the circular coordinates to be sparse, which is fundamental for analyzing geometric data of realistic size. We hope that these coordinates will be useful in problems such as the analysis of recurrent dynamics in time series data (as in [24], [23] or [7]), and nonlinear dimensionality reduction as indicated in the Experiments section 5.

An interesting direction from this work is the question of stability and Lipschitz continuity of sparse circular coordinates. The main theoretical challenge is to determine how the edge and vertex weights on the Rips complex, can be used to stabilize the harmonic cocycle representative with respect to an appropriate notion of (hopefully Hausdorff) noise on the landmark set. We hope to address this question in upcoming work.

## REFERENCES

- [1] U. Bauer. Ripser: a lean c++ code for the computation of vietoris-rips persistence barcodes. 2017. Software available at <https://github.com/Ripser/ripser>.
- [2] M. Belkin and P. Niyogi. Laplacian eigenmaps for dimensionality reduction and data representation. *Neural computation*, 15(6):1373–1396, 2003.
- [3] A. Ben-Israel and T. N. Greville. *Generalized inverses: theory and applications*, volume 15. Springer Science & Business Media, 2003.
- [4] G. Carlsson, T. Ishkhanov, V. De Silva, and A. Zomorodian. On the local behavior of spaces of natural images. *International journal of computer vision*, 76(1):1–12, 2008.
- [5] V. De Silva and G. E. Carlsson. Topological estimation using witness complexes. *SPBG*, 4:157–166, 2004.
- [6] V. De Silva, D. Morozov, and M. Vejdemo-Johansson. Persistent cohomology and circular coordinates. *Discrete & Computational Geometry*, 45(4):737–759, 2011.
- [7] V. De Silva, P. Skraba, and M. Vejdemo-Johansson. Topological analysis of recurrent systems. In *Workshop on Algebraic Topology and Machine Learning, NIPS*, 2012.
- [8] J. H. v. Hateren and A. v. d. Schaaf. Independent component filters of natural images compared with simple cells in primary visual cortex. *Proceedings: Biological Sciences*, 265(1394):359–366, Mar 1998.
- [9] D. Husemoller. *Fibre bundles*, volume 5. Springer, 1966.
- [10] I. Jolliffe. *Principal component analysis*. Wiley Online Library, 2002.
- [11] J. B. Kruskal. Multidimensional scaling by optimizing goodness of fit to a nonmetric hypothesis. *Psychometrika*, 29(1):1–27, 1964.

- [12] A. B. Lee, K. S. Pedersen, and D. Mumford. The nonlinear statistics of high-contrast patches in natural images. *International Journal of Computer Vision*, 54(1-3):83–103, 2003.
- [13] J. Milnor. Construction of universal bundles, ii. *Annals of Mathematics*, pages 430–436, 1956.
- [14] R. Miranda. *Algebraic curves and Riemann surfaces*, volume 5. American Mathematical Soc., 1995.
- [15] S. A. Nene, S. K. Nayar, H. Murase, et al. Columbia object image library (coil-20). 1996. Data available at <http://www.cs.columbia.edu/CAVE/software/softlib/coil-20.php>.
- [16] J. A. Perea. A brief history of persistence. *preprint arXiv:1809.03624*, 2018. <https://arxiv.org/abs/1809.03624>.
- [17] J. A. Perea. Multiscale projective coordinates via persistent cohomology of sparse filtrations. *Discrete & Computational Geometry*, 59(1):175–225, 2018.
- [18] M. Radovanović, A. Nanopoulos, and M. Ivanović. Hubs in space: Popular nearest neighbors in high-dimensional data. *Journal of Machine Learning Research*, 11(Sep):2487–2531, 2010.
- [19] S. T. Roweis and L. K. Saul. Nonlinear dimensionality reduction by locally linear embedding. *science*, 290(5500):2323–2326, 2000.
- [20] E. Rybakken, N. Baas, and B. Dunn. Decoding of neural data using cohomological learning. *arXiv preprint arXiv:1711.07205*, 2017.
- [21] G. Singh, F. Mémoli, and G. E. Carlsson. Topological methods for the analysis of high dimensional data sets and 3d object recognition. In *SPBG*, pages 91–100, 2007.
- [22] J. B. Tenenbaum, V. De Silva, and J. C. Langford. A global geometric framework for nonlinear dimensionality reduction. *science*, 290(5500):2319–2323, 2000.
- [23] C. Tralie and M. Berger. Topological eulerian synthesis of slow motion periodic videos. *arXiv preprint arXiv:1805.06021*, 2018.
- [24] B. Xu, C. J. Tralie, A. Antia, M. Lin, and J. A. Perea. Twisty takens: A geometric characterization of good observations on dense trajectories. *arXiv preprint arXiv:1809.07131*. <https://arxiv.org/pdf/1809.07131>.

DEPARTMENT OF COMPUTATIONAL MATHEMATICS, SCIENCE & ENGINEERING  
 DEPARTMENT OF MATHEMATICS,  
 MICHIGAN STATE UNIVERSITY  
 EAST LANSING, MI, USA.  
*E-mail address:* joperea@msu.edu